Magneto-transport phenomena in metal/SiO$_2$/n(p)-Si hybrid structures

N.V. Volkov[1], A.S. Tarasov[1,2], M.V. Rautskii[1], A.V. Lukyanenko[1,2], I.A. Bondarev[1,2*], S.N. Varnakov[1,3], and S.G. Ovchinnikov[1,2]

[1]*Kirensky Institute of Physics, Federal Research Center KSC SB RAS, Krasnoyarsk, 660036 Russia*
[2]*Institute of Engineering Physics and Radio Electronics, Siberian Federal University, Krasnoyarsk, 660041 Russia*
[3]*Siberian State Aerospace University, Krasnoyarsk, 660014 Russia*

Corresponding author e-mail: fbi1993@mail.ru; post office: Akademgorodok 50, building 38, *660036, Krasnoyarsk, Russia*

Abstract

Present review touches upon a subject of magnetotransport phenomena in hybrid structures which consist of ferromagnetic or nonmagnetic metal layer, layer of silicon oxide and silicon substrate with n- or p-type conductivity. Main attention will be paid to a number gigantic magnetotransport effects discovered in the devices fabricated on the base of the M/SiO$_2$/n(p)-Si (M is ferromagnetic or paramagnetic metal) hybrid structures. These effects include bias induced dc magnetoresistance, gigantic magnetoimpedance, dc magnetoresistance induced by an optical irradiation and lateral magneto-photo-voltaic effect. The magnetoresistance ratio in ac and dc modes for some of our devices can exceed 10^6 % in a magnetic field below 1 T. For lateral magneto-photo-voltaic effect, the relative change of photo-voltage in magnetic field can reach 10^3 % at low temperature. Two types of mechanisms are responsible for sensitivity of the transport properties of the silicon based hybrid structures to magnetic field. One is related to transformation of the energy structure of the (donor) acceptor states including states near SiO$_2$/n(p)-Si interface in magnetic field. Other mechanism is caused by the Lorentz force action. The features in behaviour of magnetotransport effects in concrete device depend on composition of the used structure, device topology and experimental conditions (bias voltage, optical radiation and others). Obtained results can be base for design of some electronic devices driven by a magnetic field. They can also provide an enhancement of the functionality for existing sensors.

Keywords: Hybrid structures, magnetoresistance, magnetoimpedance, photo-magneto-electric effect, magnetoelectronics.

Contents

1. Introduction

Multilayered hybrid structures combined from semiconductor and ferromagnetic elements are invariably considered by researchers as a main building block for semiconductor spintronics. Indeed, spin injection, spin detection, and manipulation of carriers' transport via spin statewere demonstrated in semiconductor structures with ferromagnetic electrodes of special topology [1-4]. That all is a base for building the spin transistor and, consequently, the reconfigurable digital logic for implementation of Boolean logic functions [5]. For example, the combination of the conventional metal-oxide-semiconductor field-effect transistor (MOSFET) and switchable magnetic elements allows building the plain spin field-effect transistor (SpinFET) [6]. The estimations of the device characteristics show that SpinFET can be competitive in comparison with MOSFET [5]. It is a matter of the main requirement: the small power-delay product (in other words small switching energy and short switching time). Can spin transistors, based on the hybrid structures ever satisfy other principal requirements of spin electronics? That depends on disclosure of hybrid structures potential and mainly on possibility to realize the efficient spin current manipulations. It is obvious that the most relevant problems are the search of novel hybrid structures with necessary physical properties and comprehensive study of spin-dependent phenomena in such structures.

Solving this problem, in course of experimentation we found that hybrid structures can reveal extremely unusual magneto-transport effects, which not related directly to spin dependent electron transport. We observed a number of gigantic magnetotransport effects in $M/SiO_2/n(p)$-Si based devices (where M is ferromagnetic or paramagnetic metal) hybrid structures. These effects include bias induced dc magnetoresistance (MR), gigantic magnetoimpedance (MI) including ac magnetoresistance (ac MR) and magnetoreactance (MX), dc magnetoresistance induced by an optical irradiation (Optic. MR) and lateral magneto-photo-voltaic effect (LMPE).

As long as the observed effects aren't governed by the spin or spin-dependent charge current, they apparently can't be directly used for creation of the spintronics devices. At the same time, these phenomena undoubtedly have an application potential. Indeed, the dc and ac magnetoresistive effects can be used in different magnetic sensors [7-11] and can be useful for fabricating, for example, the double-control devices that are sensitive to both magnetic field and optical radiation. In addition, it was demonstrated that simple magnetoresistive elements can be used even in magnetic-field-controlled logic for implementation of Boolean logic functions [12]. Another advantage of the silicon-based MR elements and devices, which will be discussed below, is their compatibility with CMOS technology and, consequently, the simplicity of their integration into semiconductor chips. In this way, semiconductor electronics can acquire new functional possibilities. The study of hybrid structures certainly represents self-contained scientific interest too [13], because physical mechanisms of many magnetically dependent effects are not definitely established. In present short review which certainly doesn't pretend to be complete, we intend to describe the main magneto-transport effects that we found in the $M/SiO_2/n(p)$-Si structures. In addition, we will discuss the possible physical mechanisms caused the strong sensitivity of the transport properties to the magnetic field.

2. Hybrid M/SiO₂/n(p)-Si system: Fabrication and experimental details

We studied a number of the M/SiO$_2$/n(p)-Si metal-oxide-semiconductor (MOS) structures, where M is ferromagnetic Fe [14], and Fe$_3$Si, ferrimagnetic Fe$_3$O$_4$ [15]and even paramagnetic Mn [16]. At the same time, the most interesting results were obtained for the structures with Fe and Mn layers fabricated on the silicon substrates of p- and n-types. Below we intend to discuss in detail the magnetotransport phenomena observed in these particular structures. Regarding the technology of structure fabrication, it didn't differ for cases of p- and n-type of substrates. Below, as an example, we'll describe the technology used for fabrication of the Fe/SiO$_2$/p-Si and Mn/SiO$_2$/p-Si [15, 16].

p-Si(100) wafers with a resistivity of 5 $\Omega \cdot$ cm (a doping density of 2×10^{15} cm^{-3}) were used as substrates. The substrates thickness was 350 µm. The surface of the substrate was precleaned by chemical etching and long-time annealing at temperatures of 400-650°C. This allowed us to obtain an atomically clean silicon surface. The process was monitored using high-energy electron backscattered diffraction. Then, the substrate was exposed to the aqueous solution of H$_2$O$_2$ and NH$_4$OH in the 1 : 1 : 1 ratio for 30 min at 60$^{\rm o}$C. During the exposure, a SiO$_2$ layer with the thickness of ~1.5 nm was formed on the substrate surface. The layer thickness was controlled by spectral ellipsometry.

Iron or manganese thin films were deposited at room temperature by thermal evaporation. A background vacuum of 6.5×10^{-8}Torr was used and sputtering rate was 0.25 nm/min. Thicknesses of the layers were controlled *in situ* with an LEF-751 high-speed laser ellipsometer. We obtained the structures with different film thicknesses from 5 to 20 nm.

Quality of the films was controlled by force microscopy and cross-sectional transmission electron microscopy (TEM). Atomic force images of the structure surface were taken before and after deposition of the metallic film. Roughness analysis shows that the mean surface roughness of silicon wafers with the only native SiO$_2$ layer is 0.12 nm; the roughness value for the surface of the Fe or Mn film deposited over the SiO$_2$ layer is about 0.5 nm. As we will show below, in our experiments the main processes are determined by the M/SiO$_2$/p-Si tunnel junction; therefore, the most important parameters are those, which determine quality of the M/SiO$_2$ and SiO$_2$/p-Si interfaces. Figure 1a [14] presents a TEM cross section micrograph of the Fe/SiO$_2$/p-Si structure. One can see that the structural composition includes the single-crystal silicon substrate, the amorphous SiO$_2$ layer, and the polycrystalline Fe film.

Figure 1b [16] shows a cross-sectional TEM image of the Mn/SiO$_2$/p-Si interfaces. We would like to emphasize some features of this structure. Firstly, there is no defined SiO$_2$ layer between Si and the metal film. Consequently, there are no defined Mn/SiO$_2$ and

Fig. 1. Cross-sectional TEM images of the (a) Fe/SiO$_2$/p-Si and (b) Mn/SiO$_2$/p-Si interfaces.

SiO$_2$/p-Si interfaces unlike the Fe/SiO$_2$/p-Si structure, where the SiO$_2$ layer in the cross-sectional TEM images can be clearly seen. This can be related to stronger diffusion of Mn ions in SiO$_2$ and Si as compared with diffusion of Fe ions. Secondly, the Mn film is polycrystalline and inhomogeneous in thickness. One can clearly see the two layers: lower Mn1 layer with a thickness of ~12 nm and upper Mn2 layer with a thickness of ~5 nm. For now, we cannot make any conclusion about the difference (crystal structures, morphologies, Si or other impurities, etc.) between these two layers. Thirdly, the manganese film surface is coated by a thin layer of manganese oxide MnO$_x$. Manganese was oxidized in air; the oxide film thickness is 2−3 nm.

The magnetic properties of the grown Fe and Mn films were examined using SQUID magnetometry (MPMS-5, Quantum Design) and the magnetooptical Kerr effect (NanoMOKE-2, Quantum Design). The Fe film shows the typical ferromagnetic behavior starting far above room temperature. Regarding the Mn film, there is no magnetic order and the manganese film remains paramagnetic even at the lowest temperatures (2 K), according to the data obtained.
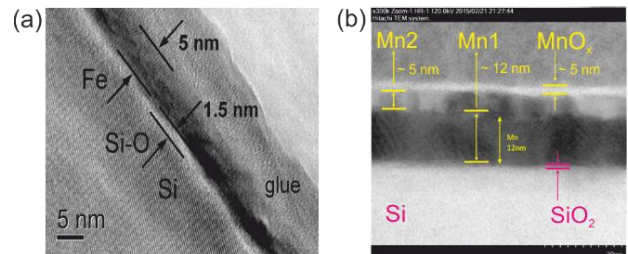
To study the main electrical properties of the structures, we fabricated MOS Schottky diodes. Transport properties of the MOS diode in ac and dc modes were studied in a two-probe configuration. One probe was attached to the top of the metallic electrode using silver epoxy and the other probe, to the substrate backside via an Al-Ga ohmic contact. The active junction area of the diodes was 1 mm. The device and measuring setup are schemati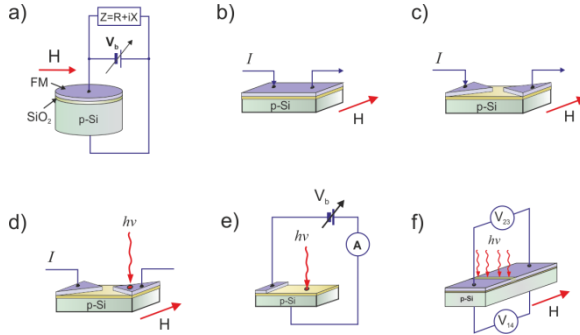cally illustrated in Fig. 2a. In dc mode, resistance and $I-V$ characteristics were measured using a precise KEITHLEY-2634 current/voltage source meter. The $I-V$ characteristics were obtained in a voltage scanning regime. Impedance spectra of the diodes were measured with an Agilent E4980A analyzer in the frequency range from 20 Hz to 1 MHz. The measuring setup allowed applying dc bias voltage V_b up to $\pm 5\,V$ across the device. The magnetotransport properties were investigated in a magnetic field applied either in the plane or along the normal to the structures. In addition to original facility based on a helium cryostat and electromagnet, we also used a Physical Property Measurement System (PPMS-9, Quantum Design) for studying the magnetotransport properties.

Fig. 2. Experimental setup for measuring of magnetotransport properties: (a) Schottky diode; (b) structure in the CIP geometry; (c) back-to-back Schottky diodes; (d) and (e) geometries for study of the photoinduced MR; (f) setup for measuring of LMPE.

To investigate the transport properties of the structures in current-in-plane (CIP) geometry, rectangles with typical sizes of 3×8 mm^2 were cut from the structure. Two types of samples were studied. The first type with continuous metallic film hereinafter referred to as the continuous-film structures. On the top of the structures, i. e., on the metallic film, Ohmic contacts were formed using two-component silver epoxy. The spacing between the contacts was 4 mm. The experimental geometry is illustrated in Fig. 2b. The second type of sample was a simplest lateral device fabricated from the structure. On the structure's surface, two electrodes separated by a gap of 20 µm were formed from a continuous metallic film (Fig. 2c). In fact, that is back-to-back Schottky diodes.

For studying MR effects induced by the optical radiation, we used the samples, which represent the back-to-back Schottky diodes (the experimental geometry is shown on the Fig. 2d) and sample with topology shown in Fig. 2e. Schematic of the sample for studying magnetic field influence on the lateral photovoltaic effect (LPE) and measuring setup are shown in Fig. 2f. The laser diodes with wavelengths of 668 and 980 nm are used as light source. Also we used the light of an incandescent lamp that was transmitted through a prismatic monochromator.

3. Magnetotransport effects: Experimental results

3.1. Bias-sensitive dc MR in CIP geometry

The first experiments on magnetic field influence on hybrid structure resistance were carried out for the Fe/SiO$_2$/p-Si structure using CIP geometry. These studies were evoked by results obtained at investigation of the LSMO/LSM$_{1-\delta}$O/MnSi tunnel structure in planar geometry [17]. The main features of the transport and magnetotransport properties are related to the current channel switching between structure layers [18].

It turned out that for the Fe/SiO$_2$/p-Si structure in CIP geometry, the current channel switching between the semiconductor substrate and the iron film occurs in the temperature range of 200-250 K [14]. This switching relates to the sharp jump in the temperature dependence of the resistance (Fig. 3).Regarding the influence of the magnetic field, the noticeable positive MR ($MR = (R(H) - R(0))/R(0)$) is observed only at high temperatures (T > 200 K), i.e., before the current channel is completely switched to the upper film. Thus, either the semiconductor volume
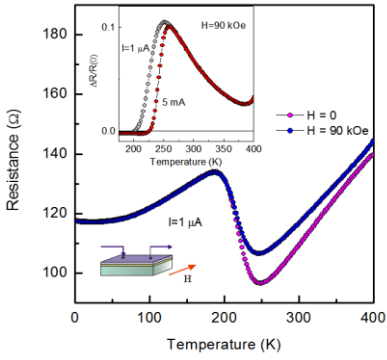
Fig. 3. Temperature dependences of the resistance of the «continues-film structure» at $H=0$ and $H=90$ kOe. The inset shows MR as a function of temperature.
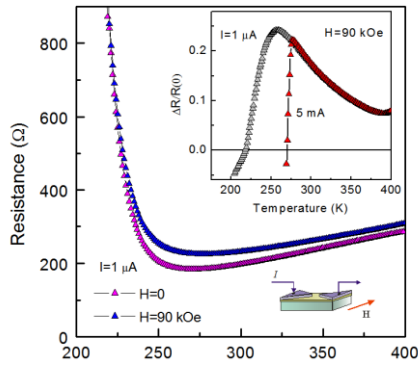

Fig. 4. Temperature dependences of the resistance of the «gap-film structure» at magnetic field $H=0$ and $H=90$ kOe. The inset shows MR as a function of temperature.
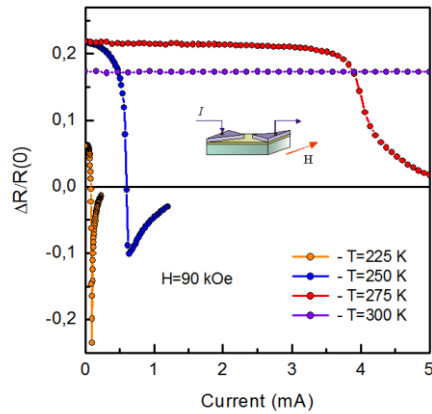

Fig. 5. Magnetoresistance of the «gap-film structure» as a function of bias current measured at various temperatures and for magnetic field $H=90$ kOe.

(p-Si substrate) or the region near SiO$_2$/p-Si interface (where Shottky barrier formed) can be responsible for MR effect.

Experimental results obtained for the gap-film structure confirm the assumption that current channel switching occurs between the semiconductor substrate and the ferromagnetic film in the continuous-film structure. As one could expect, behavior of resistance of the gap-film structure at $T>250$ K qualitatively repeats that of the continuous-film structure (see Fig. 4). However, below 250 K, R starts growing exponentially and at $T=100$ K already attains the value of about $10^5 \Omega$, which implies the rapid R growth of the Fe/SiO$_2$/p-Si tunnel junction.

The temperature dependence of MR of the gap-film structure qualitatively repeats the behavior of MR of the continuous-film structure, although quantitatively exceeds the latter more than two times. With a decrease of temperature, the monotonic growth changes to the sharp drop of MR value at the same temperatures where the sharp MR growth of the gap-film structure starts. This suggests that an MR decrease of the continuous-film structure below 250 K is not that much related to current channel switching between the substrate and the upper film, but is determined by the mechanisms responsible for the sharp growth of resistance of the Fe/SiO$_2$/p-Si tunnel junction. It is noteworthy that there is a region of negative MR at low temperatures, which was not observed for the continuous-film structure.

Moreover, while at high temperatures (the dependence at $T=275$ K in Fig. 5) MR simply approaches zero from the side of the positive values, at lower temperatures (the dependences at $T=250$ K and $T=225$ K in Fig. 5) in the transition area the portion of negative magnetoresistance appears. This portion in the $MR(I)$ dependence represents a sharp peak, which becomes more intense and narrow with decreasing of temperature. With I increasing, MR, having passed through the peak value, approaches zero. Thus, the value and even the sign of MR can be controlled by varying I value. This again allows us to conclude that origin of MR is related with Schottky barrier which, as well known, is transformed at the bias change.

3.2. Bias-controlled giant ac MR and MX effects

Involvement of the impedance and magnetoimpedance methods allows separating contribution to magnetic field sensitivity from different areas of structure. Firstly, we studied the same gap-film structure which was discussed in previous section using CIP geometry [19]. Pronounced influence of magnetic field on real (R_{ac}) and imaginary (X) parts of the impedance (z) was not observed at high temperatures. It turn out that the effect of magnetic field is strong only in the narrow temperature range of 30–50 K. In this region, the intensive peak in $R_{ac}(T)$ and the corresponding step in the $X(T)$ dependence were observed (see Fig. 6). In magnetic field, the peak becomes more intense and shifts towards higher temperatures. This explains the behavior of $MR_{ac}(T)$, specifically the presence of the portions of negative and positive magnetoresistance. The step in the $X(T)$ dependence in a magnetic field shifts to the high-temperature region (inset in Fig. 6), which causes the narrow intense peak in the $MX(T)$ dependence. By increasing frequency, the peak in the $MR_{ac}(T)$ dependence shifts towards higher temperatures, its intensity rapidly drops, but the
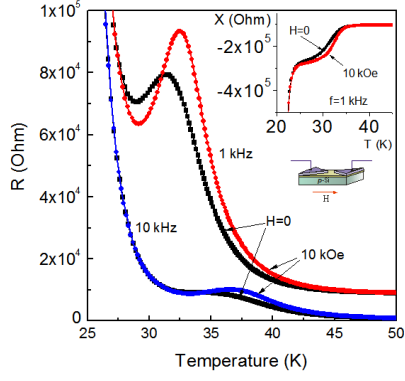
Fig. 6. Temperature dependences of the real part of impedance (R) at frequencies of 1 and 10 kHz for zero magnetic field and magnetic field of 10 kOe. Inset shows the respective behavior of the imaginary part of impedance (X).

relative change of R_{ac} in a magnetic field remains large. The same scenario is implemented for the imaginary part of the impedance.

The Schottky diode, fabricated on the n-type semiconductor substrate was found to be more convenient for study. In this case, the magneto-sensitive peaks in $R_{ac}(T)$ and corresponding steps in $X(T)$ are observed 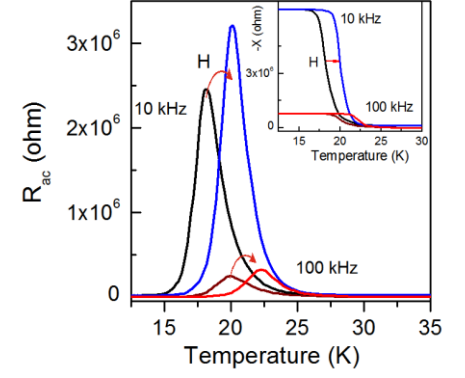in pure form [20]. The corresponding temperature dependencies for the Fe/SiO$_2$/n-Si structure are presented in Fig. 7. The variation in the $R_{ac}(T)$ in the magnetic field explains the unusual

Fig. 7. Temperature dependences of the real (main panel) and imaginary parts (inset) of the impedance at 10 and 100 kHz in zero and 1 T magnetic field.

behavior of the real part of impedance at this fixed temperature (Fig. 8a). The $R_{ac}(H)$ shape depends on the $R_{ac}(T)$ peak position at which the system is located at $H = 0$. This position is completely determined by the temperature. Figure 8a demonstrates that by choosing proper temperature, it is possible to see either positive or negative magnetoresistance or even the change in the magnetoresistive effect sign at certain H. The effect of H on the reactance is simpler (Fig. 8b): since the magnetic field caused the $X(T)$ step shift to higher temperatures, only the positive MX is realized.
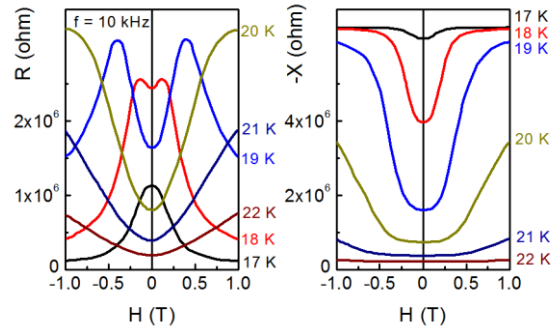
Dependence of the MR_{ac} and MX on a bias voltage across diode (V_b) shows the possibility to control sensitivity of R_{ac} and X to a magnetic field which seems to be an attractive result. Figure 9 shows that MR_{ac} and MX depend on V_b most strongly in the low-frequency region. Note here that MR_{ac} and MX ratios can reach 400-600 % in field of 1 T.

Fig. 8. (a) Real and (b) imaginary parts of the impedance versus magnetic field at different temperatures ($f = 10$ kHz).

3.3. Bias-induced giant ac and dc MR

The impedance and MI for Mn/SiO2/p-Si Schottky barrier diode reveals the same behaviour as for diode based on Fe/SiO$_2$/n-Si structure. The MI ratio does not exceed 600 % in field of 1 T. But such behaviour is observed only for low biases across diode. When forward bias exceeds the critical value V_b^c, which in our case is about 2 V (this value changes insignificantly with temperature), the behavior of the $R_{ac}(T)$ and $X(T)$ dependences and the magnetic field effect on the impedance drastically change [16]. Figure 10a shows that the peak observed in the $R_{ac}(T)$ curve at low V_b sharply changes its shape, shifts, and decreases in intensity at the biases above V_b^c. As the V_b value is increased from 0 to 5 V, the R_{ac} drops by more than five orders of magnitude. In a magnetic field, the initial peak
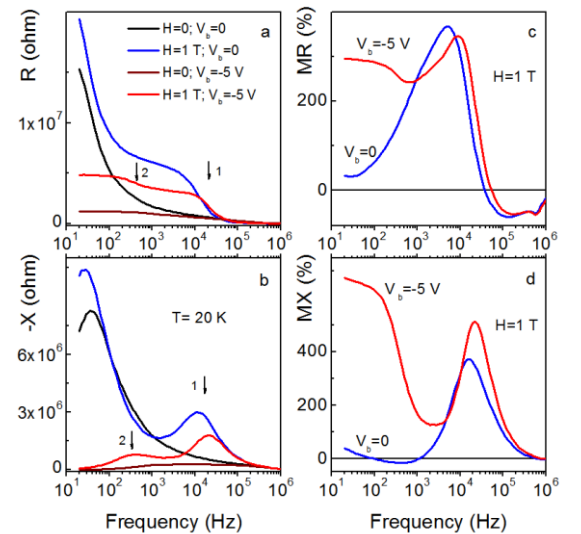

Fig. 9. (a) Real and (b) imaginary parts of the impedance vs frequency at $T = 20$ K. The dependences are recorded at zero bias and a reverse bias of -5 V in zero magnetic field and in a field of 1 T. Frequency dependences of (c) magnetoresistance and (d) magnetoreactance at zero bias and a bias of -5 V.
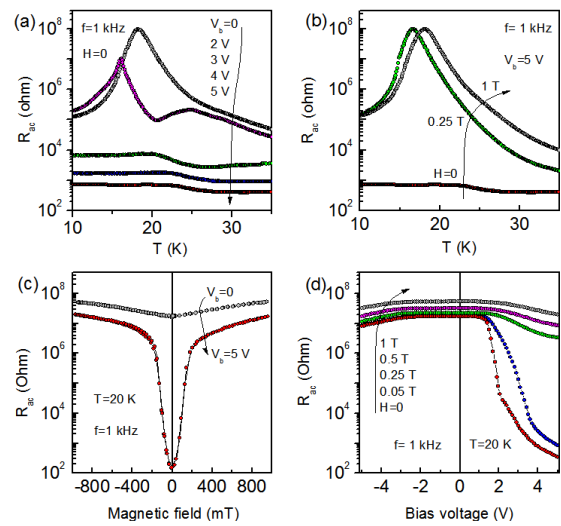
Fig. 10. Real part of the impedance (a) as a function of temperature for biases from zero to 5 V without magnetic field, (b) as a function of temperature for magnetic fields from zero to 1T at a bias of 5 V, (c) as function of magnetic field for zero bias and a bias of 5 V, and (d) as a function of bias voltage for magnetic fields from zero to 1T at T= 20 K.

size and shape rapidly recover (Fig. 10b). At that the magnetoresistance ratio increases from 200 to 10^5 %; the largest changes in R_{ac} are observed in relatively weak fields ($H < 250$ mT), see Fig. 10c. It can be seen in Fig. 10d that the magnetoresistance ratio sharply increases only at forward biases above V_b^c.

Since the largest MR_{ac} values at $V_b > V_b^c$ was observed at the lowest frequencies, it is reasonable to investigate the MR effect in the dc mode and its dependence on V_b. Recall that in the Fe/SiO$_2$/p-Si structure [18], the dc MR ratio was less than 20 % in a field of 9 T. In the Mn/SiO$_2$/p-Si structure, the dc MR effect is also insignificant at $V_b < V_b^c$, but, as can be seen in Fig. 11, at $V_b > V_b^c$ in the low-temperature region, the MR ratio can be more than 10^7 %. The strongest changes in the R value are observed even in weaker fields ($H < 100$ mT) than in the ac mode.

As was expected, the $I-V$ characteristics of the diode are nonlinear. In the temperature range of $40-300$ K, they are typical of a MOS diode with the Schottky barrier and weakly change with temperature (Fig. 12a). This confirms that in this temperature range the physical mechanisms of carrier transport remain invariable. It can be seen in Fig. 12b that below 40 K the $I-V$ characteristics become more complex and magnetic-field-sensitive. This can be related to additional low-temperature conductivity mechanisms. In zero magnetic field, when current through the diode at the forward bias attains the threshold value, it increases by few orders of magnitude. As can be seen in Figs. 12c and 12d, the effect of the magnetic field is reduced to shifting the threshold voltage at which the feature in the $I-V$ characteristics is observed. The V_b^c value rapidly grows with field and the slope of the $I-V$ curves above V_b^c remains almost invariable.

3.4. Extremely large MR induced by optical irradiation

Another effective approach for obtaining the large values of the MR ratio, as it was found out, is optical irradiation. We obtained the giant MR effect that appears under the influence of optical radiation in common planar device built on Fe/SiO$_2$/p-Si hybrid structure [21, 22]. The device represented back-to-back Schottky diodes, which was mentioned above (see Section 3.1). The optical excitation source was a laser diode with a wavelength of 980 nm and of power density (P_{opt}) up to 10 mW/cm^2. The laser was focused to a 0.5-mm spot on one MOS junction (see Fig. 2d). Photo-induced MR was positive and the MR ratio reached the values greater than 10^4 % in magnetic field of 1 T, see Fig. 13.
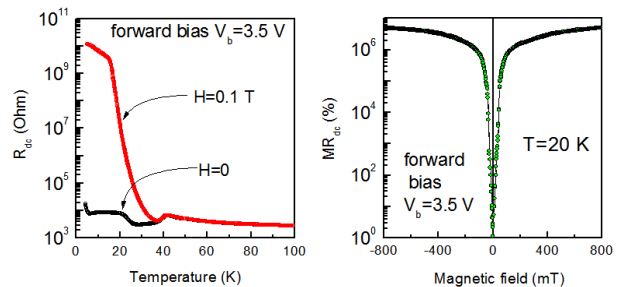

Fig. 11. (a) Temperature dependences of dc resistance at a bias of 3.5 V without magnetic field and in a field of 0.1 T. (b) Dc MR ratio as a function of magnetic field at 20 K and a bias of 3.5 V.
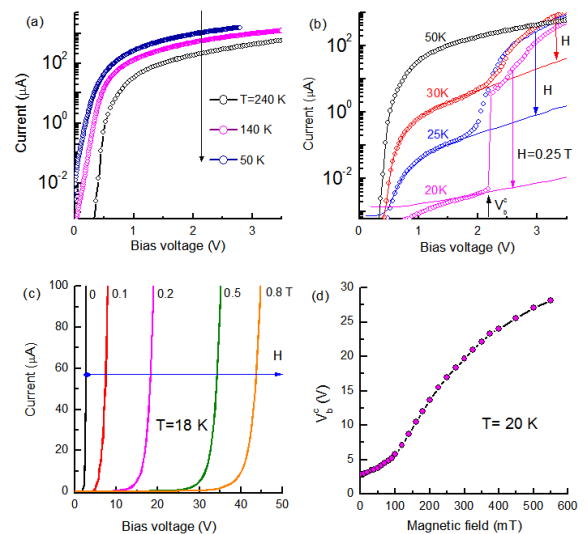

Fig. 12. $I-V$ curves (a) at $H=0$ and different temperatures above 50 K, (b) at $H=0$ (open circles) and $H=0.25$ T (solid lines) at different temperatures below 50 K, and (c) in magnetic fields of up to 0.8 T at 18 K. (d) Threshold voltage as a function of magnetic field at 20 K.
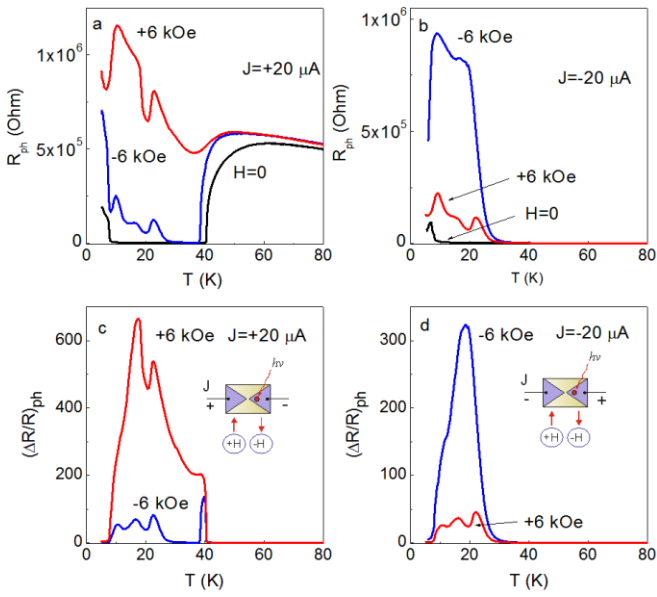
Fig. 13. Temperature dependences of the resistance under optical radiation R_{ph} at bias current of +20 μA (a) and −20 μA (b) for zero magnetic field and fields of +6 kOe and −6 kOe. Appropriate temperature dependences of the magnetoresistance $(\Delta R/R)_{ph}$ measured at positive (c) and negative (d) bias current.
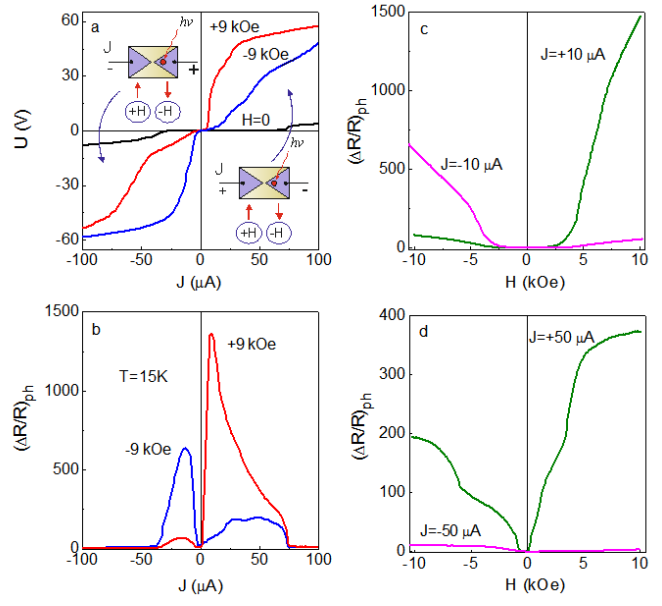
Fig. 14. (a) $I-V$ characteristics measured under optical irradiation for zero magnetic field, positive and negative fields of +9 kOe and −9 kOe. (b) Appropriate plots of the magnetoresistance $(\Delta R/R)_{ph}$ vs bias current. $(\Delta R/R)_{ph}$ as a function of magnetic field for +10 μA and −10 μA (c), +50 μA

Fig. 15. Temperature dependence of the resistance R_{ph} under optical radiation at: (a) forward bias (V_b=+2 V) and (b) reverse bias (V_b=− 2 V) for zero magnetic field, positive and negative fields of +0.6 T and − 0.6 T. Inset: schematic illustration of the device topology and the measurement setup.

The main peculiarity of the MR behavior is its strong dependence on the magnitude and the sign of the bias current across the device and, most surprisingly, upon polarity of the magnetic field.

The asymmetry of the device photo-response with respect to the sign of the bias current I and the sign of magnetic field is clearly demonstrated in $I-V$ characteristics and magnetoresistance ($(\Delta R/R)_{ph}$) dependences on I and H shown in Fig. 14. As it is mentioned geometry.

A giant change of photo-conductance in magnetic field was also observed in a Schottky-diode-like device fabricated from the Fe/SiO$_2$/p-Si structure (see inset in Fig. 15) [23]. At low temperatures the photo-conductance varies by a factor of more than 25 as the magnetic field increases up to 1 T (Fig. 15). As in case of back-to-back Shottky diodes, optically induced MR effect in the device reveals a strong dependence on polarity of applied magnetic field, sign and value of a bias voltage across the device. Thus, under certain conditions, the hybrid structures can be controlled via three parameters, namely the optical irradiation, the magnetic field and the bias voltage. It is obvious that such possibilities are of considerable technological importance.
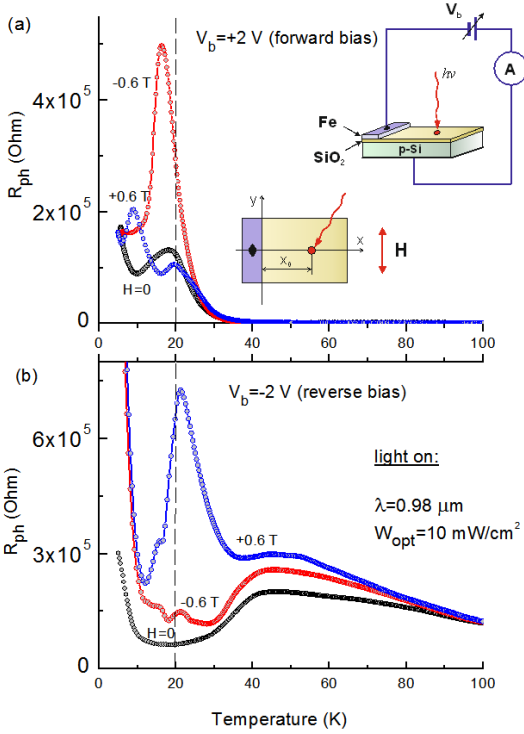
3.5. Lateral photo-magneto-voltaic effect

We demonstrate that the lateral photovoltaic effect in the Fe/SiO$_2$/p-Si structure, observed both on the Fe film and Si substrate sides (see Fig. 2f), not only depends strongly on the optical radiation wavelength and temperature, but is also sensitive to external magnetic fields [24]. Magnetic field lowers the absolute value of lateral photovoltage (PV) regardless of the wavelength and temperature (Fig. 16a); however, the relative photovoltage variation significantly depends on these parameters (Fig. 16b). A value of relative photovoltage change, which we define as $MV = (PV(H) - PV(0))/PV(0)$, in magnetic field of 1 T does not exceed 10-20 %. At that, the increasing of P_{opt} results to suppression of LMPE.

But such behavior is observed only for high temperatures ($T > 30$ K). Much stronger and more complicated magnetic field influence on lateral PV is observed at low temperatures ($T > 30$ K). Below 30 K PV decreases and changes sign near 12 K, but MV variation (increasing) reaches 10^4 % in a field of 1 T (Fig. 17). The dependence of MV on P_{opt} is also nontrivial. In particular, by changing P_{opt} one can both change MV value and switch signs of PV and MV.

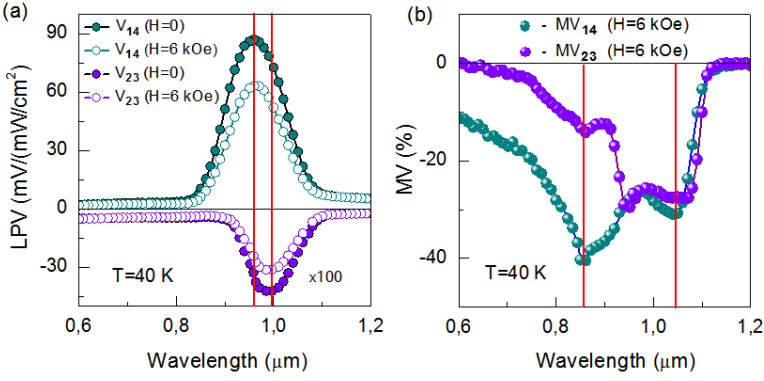## 4. Magnetotransport effects in hybrid structures with Schottky barrier: Physical mechanisms

Fig. 16. (a) LPV measured on the Si and Fe surfaces as a function of light wavelength ($V_{14}(\lambda)$ and $V_{23}(\lambda)$, respectively); the dependences are measured in fields of $H = 0$ and $H = 6$ kOe at $T = 40$ K. (b) LPME ratio as a function of light wavelength ($MV_{14}(\lambda)$ and $MV_{23}(\lambda)$, respectively).

The detail analysis of all observed magnetotransport phenomena showed the necessity to attract some different physical mechanisms for their explanation. Let us discuss the main of them which, from our point of view, determine the high sensitivity of transport properties of the devices fabricated from silicon based hybrid structures to magnetic field. These mechanisms can be tentatively grouped in four types.

4.1. Mechanism originated from interface states

First group of magnetoresistance effects relates to interface states which are located near interface within Schottky barrier. In fact, these interface states are the acceptor centers in case of the p-type semiconductor (the donor centers in case of n-type semiconductor), the energy levels of which are pinned to certain point in the semiconductor band gap at the SiO_2/Si boundary. It is found, that the recharge of such states (see Fig. 18) is completely responsible for the low temperature features in impedance behavior and for appearance of magneto-impedance. Let us remind that all change of z in magnetic field takes place only in range of the low temperature features. Application of magnetic field causes shift of the peak in the $R(T)$ dependence and corresponding step in $X(T)$ dependence. In the MOS structures, these features are caused solely by a delay in recharging of the interface states localized near the insulator/semiconductor interface [25]. Those recharge processes may be affected by the ac-measurements since voltage V_{ac} applied to the MOS structure swept the Fermi level through the interface center energy levels (Fig. 19). The $R(T)$ peak should occur under the condition $\omega\langle\tau\rangle = 1$, where $\omega = 2\pi f$ is the angular frequency of V_{ac} and $\langle\tau\rangle$ is the average relaxation time that characterizes the charge-discharge process at the interface. In general, the relaxation time is $\tau = \tau_0 \exp(E_s/k_B T)$, where E_S in case of n-type semiconductor is the interface state energy relative to the bottom of the conduction band (E_C), and τ_0 is the prefactor determined by the electron capture cross-section, density of states in the conduction band, degeneracy factor of the interface states, the tunneling probability and the density of states in the metal electrode.

As was illustrated, the MI phenomenon in the MOS Fe/SiO_2/n-Si diode structure should be considered in terms of the magnetic field effect on energy spectrum of states at the SiO_2/n-Si interface [20]. E_S shifts towards E_C, therefore Fermi
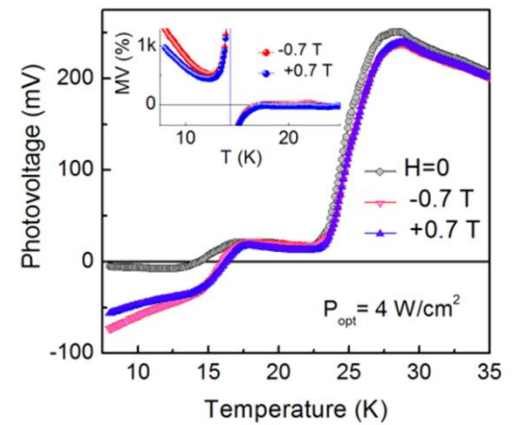

Fig. 17. (a) Schematic experimental set-up for measuring of LPE and LMPE. (b) LPV as a function of temperature at magnetic fields of H=0, -7 and +7 T. Inset: temperature dependences of LMPE ratio evaluated from LPV dependencies.
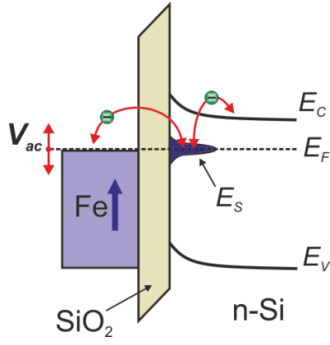
Fig. 18. Schematic illustration of the recharging process for interface states at applying ac voltage across MOS structure.

level crosses the energy levels of the interface states at higher temperatures than it would do without field. As a result, the $R(T)$ peak and $X(T)$ step in the field are also observed at higher temperatures.

Positions of the surface states energy levels in the band gap and E_S in magnetic field can be roughly estimated with the use of the simple relation $\ln(\omega) = \ln\left(1/\tau_0 - E_S/(k_B T)\right)$, where T_p is the $R(T)$ peak position at fixed ω. For simplicity, we assume τ_0 to be independent of T. Fitting the experimental $\ln(\omega)$ dependence by a straight line E_C was estimated from the line slope; the intercept gives the value of τ_0. Such a plot is shown in Fig. 20 for the data obtained at $H = 0$ and $H = 1$ T. Thus obtained positions of E_S in zero and nonzero fields are 37.8 meV and 42.0 meV relative to E_C, respectively. The value of τ_0 remains nearly independent upon the applied magnetic field, which indicates that field has very weak effect on parameters such as: capture coefficient, tunneling probability, and densities of states in the metal and semiconductor conduction band.
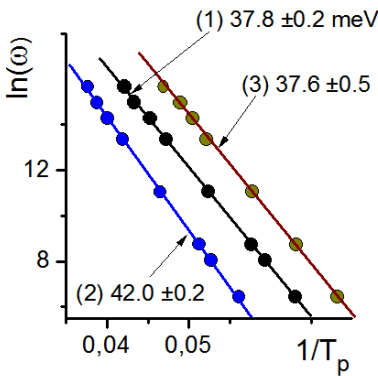
The shift of energy levels of the surface states in magnetic field (ΔE_S^H) appeared to be surprisingly large: 4 meV. For comparison, the value of Zeeman splitting of the levels does not exceed 0.06 meV at $S = 1/2$ in a field of 1 T. The final conclusion about origin of this behavior will be made after establishing the nature of the interface states and determining the mechanisms of magnetic field effect on their energy structure. By now, these questions remain unanswered. It is only possible to state, that magnetic field influence results to shift of the energetic

Fig. 19. Schematic band diagram of the Fe/SiO₂/n-Si Schottky diode, which illustrates shift of the interface state levels in magnetic field.

levels of the centers relatively to Fermi level. As a result, the recharging process is modified and transport properties are also change.

How the bias voltage affects MI? It is well-known that by varying V_b across the MOS structure, the position of the energy levels of the interface states changes according to shift of the semiconductor band gap edges, whereas the position of the Fermi level remains invariable (Fig. 21). It was found that in the case of Fe/SiO₂/n-Si diode, application of reverse bias $V_b < 0$ causes shift of $R(T)$ peaks and corresponding $X(T)$ steps toward lower temperatures. Similar analysis described above (Fig. 20) showed that at $V_b < 0$ up to −5 V, there was no noticeable variation of E_S (E_S was invariable within the measurement error), while τ_0 changed.

Fig. 20. Dependence of $\ln(\omega)$ vs $1/T_p$ reciprocal peak temperature for determining energy levels, E_S, of the interface states. (1) - $H = 0$, $V_b = 0$; (2) - $H = 1$ T, $V_b = 0$; (3) - $H = 0$, $V_b = -5$ V.

What is the reason of strong influence of bias on MI mainly in low frequency region (see Fig.9)? Here, one should take into account the magnetic field effect on the electron tunneling probability between centers and ferromagnetic electrode. Actually, at low frequencies the interface states are recharged by a certain sequence of the capture-emission processes, involving conduction band and electron tunneling through potential barrier [20]. At higher frequencies, only the direct capture-emission process is realized. Of course, that is only speculation, but the physical mechanism of the bias effect on MI is yet to be figured out.
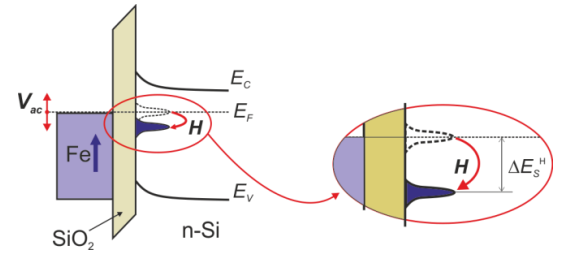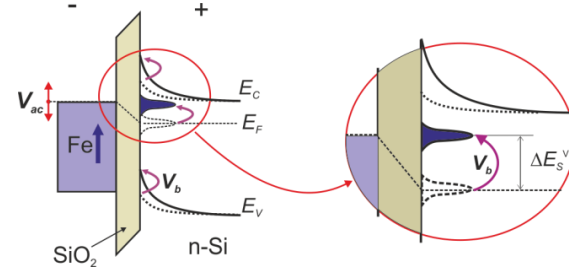

Fig. 21. Change of band diagram of the Fe/SiO₂/n-Si Schottky diode with applying bias voltage.

10

4.2. Magnetotransport effects governed by impact ionization process

To explain certain magnetotransport phenomena, it is necessary to attract the impact ionization process. Usually this process occurs at high biases when carriers gain sufficient kinetic energy. Let us consider the anomalously strong magnetotransport effects which are attributed to the magnetic-field-dependent impact ionization process by example of a Mn/SiO$_2$/p-Si based diode with the Schottky barrier (see Section 3.3) [16].

The main parameter determining the behavior of diode transport properties at the temperatures $T < 40$ K is hole density n in the bulk of the Si substrate. Around 40 K, E_F becomes lower than E_A and acceptor states in p-Si start to trap holes intensively. The majority carrier density starts dropping with temperature, which leads to a rapid decrease of current through the structure. Below 40 K the $I-V$ characteristics change abruptly when a bias voltage reach V_b^c. Sharp current growth above the threshold voltage and the main features of the transport properties at $V_b > V_b^c$ are related to the autocatalytic impact ionization process of the shallow acceptor boron in bulk of the semiconductor. When high bias voltage is applied, carriers acquire kinetic energy, which exceeds the ionization energy of acceptor impurities; i.e., impact ionization occurs. Since the ionization energy ($\sim E_A$) is only about 40 meV, the breakdown already occurs in fields of few V/cm and lasts until all impurities are ionized.

What is the mechanism of a magnetic field effect in this case? As we already shown during the structure impedance study, in magnetic field the E_A value shifts to the high-energy region by ΔE_S^H. Qualitatively, it is obvious that enhancement of E_A relative to valence band leads to the growth of impact ionization activation energy; i.e., the process will be initiated at large electric field F (and V_b, respectively) (Fig. 22a). Using the balance equation for a kinetic process, which determines the hole density in a certain F (V_b) it is possible to show that V_b exponentially depends on the acceptor level depth [26], i.e., $\Delta V_b^c \sim \exp\left(\Delta E_A^H / (k_B T)\right)$. This fact, namely, determines strong dependence of $I-V$ characteristics on magnetic field and therefore resultant giant MR effect.

Considered mechanism of magnetic field effect on impact ionization process is not unique. We can expect the same order-of-magnitude magnetic field influence due to the Lorentz force effect. In external magnetic field, carrier trajectories are deflected by the Lorentz force, which increases the probability of inelastic scattering, decreases the kinetic energy of carriers and, as a result, suppresses impact ionization (Fig. 22b). To restore the impact ionization process, a greater electric field (and V_b, respectively) is required; in other words, magnetic field increases the threshold voltage of the current breakdown [27]. In the classical consideration, under the assumption of parabolic band dispersion, in the weak magnetic field approximation, we can obtain the quadratic dependence of V_b^c on H [28]: $\Delta V_b^c \sim \alpha H^2$, where α is a parameter which depends on acceptor levels position, carrier effective mass and mobility, and some other physical quantities.

Simple estimations show that the described Lorentz force-related mechanism explains well the experimentally observed growth of V_b in a magnetic field. In this case, the $V_b^c(H)$ curve initially has quadratic form, indeed. In strong magnetic fields, the reason of deflection is obvious: the approximations and simplifications were used and quadratic dependence stopped working. Considering this mechanism the observed anisotropy of the magnetic field effect becomes clear: transport properties change mostly in a magnetic field perpendicular to the current, whereas in a magnetic field parallel to the current, the transport properties are negligibly affected by the field.
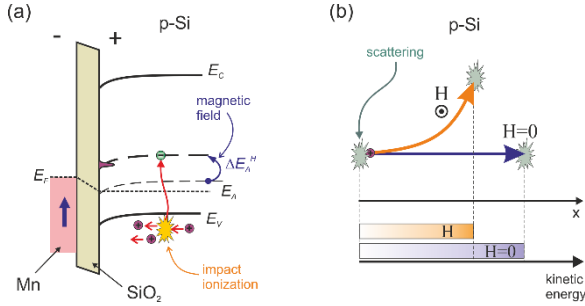

Fig. 22. Schematic diagrams illustrating magnetic field influence on impact ionization process. (a) Shift of the acceptor levels leads to increase of the activation energy for impact ionization. (b) Deflection of carrier trajectory in magnetic field suppresses acquisition of kinetic energy between scatterings.

Above we discussed how the impact ionization process provides the appearance of the giant dc MR. A question arises: How does the impact ionization leads to the giant MI effect as well? After all, we know that all features of the impedance at low temperatures, where the giant MI effect occurred, are related to surface states formed at the SiO_2/Si boundary rather than the acceptor states in a volume of the semiconductor substrate. The point is that the impact ionization results to full ionization of both the acceptor levels in p-Si and the surface states which completely suppresses recharging of the latter and leads to the sharp impedance drop. Suppression of impact ionization by magnetic field rapidly recovers large impedance values and, thus, leads to the large MI ratio.

Regarding the large MR and MI effects related impact ionization in the hybrid structures, we cannot yet explain what role is played by dielectric barrier, Schottky barrier, and metal electrode material. Meanwhile, judging by our data and data obtained by other authors, this item is of principle importance. To date, we can only state that they assist the autocatalytic process of impact ionization and determine the conditions of its triggering.

4.3. MR defined by the Lorentz force

MR effects in systems with nonequilibrium charge carriers can also be explained by attracting not only one mechanism but the combination of the different ones. As an example, let us discuss the giant change of the photoconductivity in magnetic field which is observed in a Fe/SiO_2/p-Si based device [23]. In this case, a magnetic field affects the transport of nonequilibrium charge carriers induced by an optical radiation (see Section 3.4). Here, on one hand, the main mechanism derives from Lorentz force, but on the other hand, the magnetic field influence on the interface states at the SiO_2/Si boundary also gives considerable contribution in MR effect.

The Lorentz force deflects the trajectories of the photo-generated charge carriers moving in the electric field thereby changing a velocity of their recombination (Fig. 23). Structural asymmetry of the device leads to an asymmetry in the dependence of recombination on the magnetic field polarity: relatively slow recombination occurs for the carriers deflected in a volume of semiconductor, on the contrary for carriers near SiO_2/p-Si interface recombination is strengthened. In the last case, the interface states act as effective recombination centers. Recombination rate depends on the carrier type (electron or hole) and also on the centers' charge state, i.e. depend on the Fermi-level position with respect to the centers energy levels. In particular, the rate of holes recombination on the interf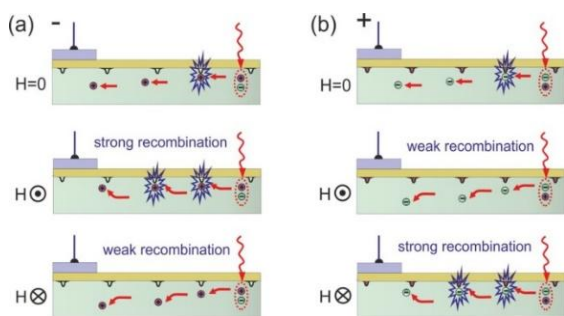ace centers is higher when their energies approach the Fermi level E_F. Thus, magnetic field can influence on transport of nonequilibrium charge carriers by changing the energetic state of the interface centers.

Sign of the bias voltage specifies the type of carriers passing near the interface which provide the main contribution to MR effect. Value of bias voltage sets electric field which accelerates charge carriers, thus it affects the hole and electron trajectories, in similar way as magnetic field.

Summing up the above, we can conclude that at least two mechanisms are responsible for the MR effects in a device with nonequilibrium optically induced carriers. Those are Lorentz force effect and shift of the interface center levels in magnetic field. Unfortunately, it is impossible to separate these contributions for the time being.

Fig. 23. Schematic illustration of photo-generated charge carriers transport in the device without magnetic field and in magnetic field of two different polarities at (a) forward and (b) reverse bias voltages. Magnetic field deflecting carriers towards the interface which lead to strengthening of recombination due to the interface states.

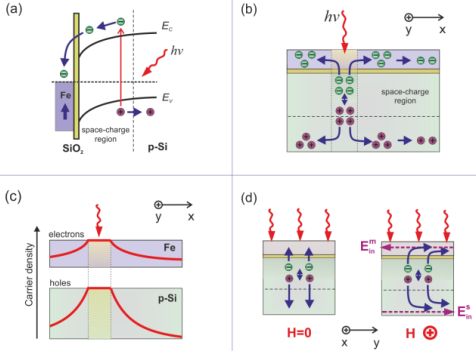## 4.4. The Schottky barrier change at combined exposure of magnetic field and optical radiation

Fig. 24. (a) Schematic energy-band diagram of the MOS junction demonstrates the process of the electron-hole pair separation due to Schottky field. (b) The picture illustrates the origin of LPV as a result of electron-hole pair separation and lateral carrier diffusion. (c) Schematic diagram of stationary distribution of electron and hole densities on surface of Fe film and Si substrate. (d) The picture illustrates the origin of the LPMEE due to Lorentz forces which deflect carriers resulting thereby to suppression of LPV.

It is turn out that simultaneous exposure of magnetic field and optical radiation can result to change of Schottky barrier parameters and, consequently, to change of the charge carrier transport in hybrid structures. Such situation is realized, for example, in the effect of magnetic field influence on LPE. The mechanism of the LPV generation in structures with Schottky barrier is illustrated in (Fig. 24). The optical radiation absorbed in the p-Si substrate generates electron-hole pairs. Generated electrons and holes are instantaneously separated by a strong electric field $\varepsilon(z)$ (Schottky field) in the depletion (space-charge) region. Electrons in the depletion region of the structure and within approximate diffusion length are swept into the Fe layer by the Schottky field, at the same time holes are swept into the substrate volume. Under irradiation of the local substrate area, the separation process results in the carrier density gradient between the illuminated and unilluminated regions. Under irradiation of local area of the substrate, such separation process result in carrier density gradient between the illuminated and nonilluminated zones. That forces excess electrons in metal and excess holes in the semiconductor to diffuse laterally from the illuminated zone. Obviously, if the lateral distances from the electrodes in the illuminated area are different, the carrier densities at the electrodes are different, too. As a result, the potential difference (LPV) arises between the electrodes.

Regarding magnetic field influence on LPV, it behavior strongly differs at low and high temperatures (above and below 30 K) for Fe/SiO$_2$/p-Si structure, (see Section 3.5). At high temperatures, the magnetic field influence is purely related to Lorentz force. Magnetic field deflects the trajectory of charge carriers which drift in transverse direction due to an effect of $\varepsilon(z)$. Lengthening of the trajectories results to increasing of the recombination probability of the nonequilibrium charge carriers and, finally, to decreasing of LPV.

Why does an increase of P_{opt} result to LMPE suppression? The reason of that can be the change of band bending at the p-Si interface under light illumination [29]. Obviously, it is equivalent to change of $\varepsilon(z)$. For qualitative understanding of the mechanism, let us consider a simple idealized case of the Schottky barrier forming [30]. Relation between $\varepsilon(z)$ and electric potential ($\psi(z)$) is given by the one-dimensional Poisson equation $\partial^2\psi(z)/\partial z^2 = -\rho(z)/\varepsilon_s$, where $\rho(z)$ is the total space charge density and ε_s is the permittivity of semiconductor. In the Schottky barrier space-charge region for the p-type semiconductor electrical charge originates from charge of the ionized acceptors with density of N_A^-, the electron ($n_p(z)$) and hole ($p_p(z)$) densities $\rho(z) = q\left(-N_A^- + p_p(z) - n_p(z)\right)$, where q is an elementary charge. $n_p(z)$ and $p_p(z)$ are connected by

Fig.25. (a) Band alignment of the structure in the dark and under illumination. The absorption of the light in space-charge region induces the flattening of the band bending due to mobility difference for the electrons and holes. (b) Fragment of the energy diagram of the structure at low temperature under illumination without and in a magnetic field. The field shifts the acceptor levels that also results to the flattening of the band bending.

specified relations with $\psi(z)$ [30], it is fundamentally that values of $n_p(z)$ and $p_p(z)$ under optical radiation will differ from values in equilibrium conditions, i.e., $\rho(z)$ becomes a function of P_{opt}. That is provided by the difference in the drift and diffusion velocities of the nonequilibrium holes and electrons which results in turn to dissimilar change of $n_p(z)$ and $p_p(z)$.

At high temperatures, $E_A < E_F$ and N_A^- is a constant, but optical radiation results to decreasing of $n_p(z)$ due to photoexcitation of the electrons and their further tunneling into a metal. At the same time, nonequilibrium density $p_p(z)$ grows. Such change of $\rho(z)$ decreases $\psi(z)$ in space-charge region (see Fig. 25(a)) and, respectively, decreases $\varepsilon(z)$ ($\varepsilon(z) = -d\psi/dz$) which initiates the drift motion of charge carriers. It is clear that the magnetic field influence on LPV will decrease due to the decrease of carriers' drift speed, and thereby, decrease of Lorentz force. That is observed in experiment.

At low temperatures magnetic field influence is explained by shift of E_A towards higher energies, including states near the interface. This question was narrowly discussed above. Considering this, the mechanism of low temperature LPE behavior in magnetic field can be following. In magnetic field, the E_A levels shift and become higher than E_F for an increasing number of acceptor states near the interface (see Fig. 25(b)), i.e. the N_A^- effectively decreases and so does the field $\varepsilon(z)$. Relative contribution of diffusion current inside the semiconductor increases – we can see the increase of LPV from Si side, caused by non-equilibrium electrons.

5. Summary

All discussed structures and devices, where giant MR effects are present, has two common features – Schottky barrier and surface states levels. Comparing, for example, ac MR values for MOS diodes with ferromagnetic and nonmagnetic metal layer (Table 1), one can notice, that magnetic state of metal electrode doesn't have a determining influence on effect. Furthermore, MR value in $Mn/SiO_2/p$-Si diode exceeds the corresponding value in $Fe/SiO_2/p$-Si and $Fe/SiO_2/n$-Si by three orders of magnitude due to the impact ionization process. It also should be noted, that MR value depends on the device type. In case of $Fe/SiO_2/p$-Si structure highest MR effect is observed in back-to-back diode. And using optical irradiation for generation of photo-generated charge carriers, one can achieve a significant increase of MR in comparison to ac or dc modes.

It's important to note, that the maximal MR is observed under noneqillibrium conditions such as optical irradiation and impact ionization process. In this conditions transport current or voltage is highly sensitive to carriers' concentration. So, it is clear that maximal device sensitivity to magnetic field appears when magnetic field affects carriers' concentration one way or another. This can be achieved via different methods for different structures and devices, exploiting the shifting of surface states levels in magnetic field and/or device topology.

Table 1. Values of MR effects observed in $M/SiO_2/n(p)$-Si hybrid structures.

Structure composition	Device type	Effect		
		dc MR, %	ac MR, %	Optic. MR, %
$Fe/SiO_2/p$-Si	film	+ 10 % at 9 T	-	$+10^4$ % at 1 T (photovoltage)
	back-to-back diode	± 20 % at 9 T	± 100 % at 1 T	$+ 10^4$ % at 1 T
	diode	-	-	2500 % at 1 T
$Fe/SiO_2/n$-Si	diode	-	± 500 % at 1 T	-
$Mn/SiO_2/p$-Si		$+ 10^7$ % at 0.1 T	$+ 10^5$ % at 0.2 T	-

6. Conclusions

$M/SiO_2/p(n)$-Si hybrid structures with Schottky barrier reveal the variety of magnetotransport effects. Some of these effects reach giant values. There are two fundamental

mechanisms which are responsible for ac and dc magnetoresistance. The first is shifting of acceptor (donor) levels and surface states levels at the $SiO_2/p(n)$-Si interface, caused by magnetic field. The strongest response is observed at low temperatures, when Fermi level is equal to surface states levels and acceptor (donor) levels. The second mechanism is related to Lorenz force action on charge carriers. It can lead, for example, to surpassing of impact ionization process or to an increase of recombination probability in a case of non-equilibrium carriers. This MR mechanism works in almost all temperature range, from helium to room temperatures, though it doesn't provide large MR values. However, it is possible to combine two mentioned mechanisms, like when charge carriers deflect to the surface, where surface states work like active recombination centers.

We think that the discussed mechanisms of giant magnetotransport phenomena can become the basis for design of the novel class of CMOS technology-compatible magnetoresistive devices. We already suggested and patented the magnetic sensor, based on GMI effect [31]. And discovery of the lateral photo-magneto-electric effect gives hope to expand functionality of position-sensitive detectors, based on the lateral photovoltaic effect –it can be magnetic field-controlled detectors or double-control sensors, which will allow controlling both optical and magnetic parameters. Another effects discovered in our work can also find application in sensors.

References

1. Y. Ando, K. Hamaya, K. Kasahara, Y. Kishi, K. Ueda, K. Sawano, T. Sadoh, and M. Miyao. Appl. Phys. Lett. 94 182105 (2009).
2. Y. Ando, Y. Maeda, K. Kasahara, S. Yamada, K. Masaki, Y. Hoshi, K. Sawano, K. Izunome, A. Sakai, M. Miyao and K. Hamaya. Appl. Phys. Lett. 99 132511 (2011).
3. S. Takahashi and S. Maekawa. Sci. Technol. Adv. Mater. 9 014105 (2008).
4. S.P. Dash, S. Sharma, R.S. Patel, M.P. de Jong, and R. Jansen, Nature (London) 462 491 (2009).
5. D.E. Nikonov and I.A. Young. Overview of Beyond-CMOS Devices and A Uniform Methodology for Their Benchmarking Proceedings of the IEEE, v.101, Is.: 12,pp. 2498 - 2533 (2013) DOI: 10.1109/JPROC.2013.2252317
6. S. Sugahara and M. Tanaka. A spin metal-oxode-semiconductor field effect transistor using half-metallic-ferromagnet contacts for the source and drain. Appl. Phys. Lett. 84 (13) 2307 (2004)
7. A. Fert. Phys. Usp., **51** 1336 (2008).
8. H. Kaiju, S. Fujita, T. Morozumi, and K. Shiiki, J. Appl. Phys. 91, 7430 (2002).
9. T.Y. Peng, S.Y. Chen, L.C. Hsieh, C.K. Lo, Y.W. Huang, W.C. Chien, Y.D. Yao, J. Appl. Phys. 99, 08H710 (2006).
10. R.S. Beach, N. Smith, C.L. Platt, F. Jeffers, and A.E. Berkowitz, Appl. Phys. Lett. **68**, 2753 (1996).
11. M.H. Phan and H.X. Peng, Prog. Mater. Sci. 53, 323 (2008).].
12. S. Joo, T. Kim, S.H. Shin, J.Y. Lim, J. Hong, J.D. Song, J. Chang, H.-W. Lee, K. Rhie, S.H. Han, K.-H. Shin and M. Johnson. Nature 494, 72-76 (2013).
13. R. Jansen, Nature Materials **11** 400 (2011).
14. N.V. Volkov, A.S. Tarasov, E.V. Eremin, S.N. Varnakov, S.G. Ovchinnikov, and S.M. Zharkov, J. Appl. Phys. 109, 123924 (2011).
15. A.S. Tarasov, M.V. Rautskii, A.V. Lukyanenko, M.N. Volochaev, E.V. Eremin, V.V. Korobtsov, V.V. Balashev, V.A. Vikulov, L.A. Solovyov, N.V. Volkov. Magnetic, transport, and magnetotransport properties of the textured Fe_3O_4 thin films reactively deposited onto SiO_2/Si. Journal of Alloys and Compounds, **688**, 1095-1100 (2016)
16. N. V. Volkov, A. S. Tarasov, D. A. Smolyakov, A. O. Gustaitsev, M. V. Rautskii, A. V. Lukyanenko, M. N. Volochaev, S. N. Varnakov, I. A. Yakovlev, and S. G. Ovchinnikov Extremely high magnetic-field sensitivity of

charge transport in the Mn/SiO2/p-Si hybrid structureю. AIP Advances **7**, 015206 (2017); doi: 10.1063/1.4974876

17. N.V. Volkov, E.V. Eremin, V.S. Tsikalov, G.S. Patrin, P.D. Kim, Yu Seong-Cho, Dong-Hyun Kim, and Nguyen Chau. Current-driven channel switching and colossal positive magnetoresistance in the manganite-based structure, J. Phys. D: Appl. Phys. Vol. 42, 065005 (6pp), (2009).

18. N.V. Volkov. Spintronics: manganite-based magnetic tunnel structures Physics-Uspekhi 55 (3) 250-269 (2012)

19. N. V. Volkov, A. S. Tarasov, E. V. Eremin, A. V. Eremin, S. N. Varnakov, and S. G. Ovchinnikov. Frequency-dependent magnetotransport phenomena in a hybrid Fe/SiO2/p-Si structure // Journal of Applied Physics, v.112, 123906 (2012).

20. N.V. Volkov, A.S. Tarasov, D. A. Smolyakov, A.O. Gustaitsev, V.V. Balashev, and V.V. Korobtsov. The bias-controlled giant magnetoimpedance effect caused by the interface states in a metal-insulator-semiconductor structure with the Schottky barrier // APPLIED PHYSICS LETERS 104, 222406 (5 pp) (2014).

21. N.V. Volkov, A.S. Tarasov, E.V. Eremin, F. A. Baron, S.N. Varnakov, and S.G. Ovchinnikov. Extremely large magnetoresistance induced by optical irradiation in the Fe/SiO2/p-Si hybrid structure with Schottky barrier // JOURNAL OF APPLIED PHYSICS **v.114**, 093903(8pp) (2013).

22. N.V. Volkov, A.S. Tarasov, D.A. Smolyakov, S.N. Varnakov, S.G. Ovchinnikov. Bias-voltage-controlled ac and dc magnetotransport phenomena in hybrid structures // Journal of Magnetism and Magnetic Materials **383,** pp.69–72 (2015).

23. N.V. Volkov, A.S. Tarasov, M.V. Rautskii, A.V. Lukyanenko, et al., The optically induced and bias-voltage-driven magnetoresistive effect in a silicon-based device, J. Surf. Invest. X-Ray, Synch. Neutron Tech. 25 (5), 984 (2015). URL:http://link.springer.com/article/10.1134/S1027451015050432, doi: 10.1134/S1027451015050432.

24. N.V. Volkov, A.S. Tarasov, M.V. Rautskii, A.V. Lukyanenko, S.N. Varnakov, S.G. Ovchinnikov. Magnetic-field-driven electron transport in ferromagnetic/ insulator/ semiconductor hybrid structures // JMMM 440 140–143 (2017)

25. D. L. Losee, J. Appl. Phys. **46**, 2204 (1975).

26. M.E. Cohen and P.T. Landsberg. Effect of Compensation on Breakdown Fields in Homogeneous Semiconductors // Phys. Rev.v.154 (3) 683 (1967).

27. S. Salahuddin. Nature 494 43 (2013)

28. J. Hong, T. Kim, S. Joo, J. D. Song, S. H. Han, K.-H. Shin, J. Chang. Preprint at arxiv.org/abs/1206.1094v1 (2012)

29. Wei Jin Hu, Zhihong Wang, Weili Yu & Tom Wu. Optically controlled electroresistance and electrically controlled photovoltage in ferroelectric tunnel junctions. NATURE COMMUNICATIONS | DOI:10.1038/ncomms10808

30. S.M. Sze, Kwok K. Ng. Physics of Semiconductor Devices. 3rd ed. (John Wiley & Sons, Inc., Hoboken, New Jersey, 2007)

31. D.A. Smolyakov, N.V. Volkov, A.O. Gustaitsev, A.S. Tarasov, Sensitive element based on magnetoimpedance. RF patent №2561232 (2015).